Correction published 1 December 2007

Intermediate MHD shocks with a terrestrial magnetopause*

S. Cable,[1] Y. Lin,[2] and J. L. Holloway[3]

Received 23 March 2007; revised 30 May 2007; accepted 12 June 2007; published 8 September 2007.

[1] Previous MHD simulations predict that when switch-on shock conditions obtain in the solar wind, the bow shock produced in front of an ellipsoidal obstacle will produce a unique bow shock configuration that includes a concave intermediate shock region at the nose of the shock. These simulations have been carried out with hard shell inner boundary conditions. We extend these studies by investigating the configuration of the bow shock when the obstacle is a terrestrial magnetic dipole field. It is found that, in contrast to the typical fast shock, reconnection at the magnetosphere affects the structure of the upstream magnetosheath and bow shock considerably. Asymmetry in magnetic reconnection rates between the northern and southern hemispheres changes the bow shock configuration notably. In the hemisphere where the dipole field is largely antiparallel to the interplanetary magnetic field, the intermediate shock is eliminated in favor of a standard fast shock. In the other hemisphere, however, the intermediate shock still forms as an important, stable element of the overall shock configuration. We also launch a solar wind MHD fast shock into the simulation domain and observe how the resulting waves transmit and reflect in the magnetosheath and magnetosphere and how the general morphology of the bow shock changes.

Citation: Cable, S., Y. Lin, and J. L. Holloway (2007), Intermediate MHD shocks with a terrestrial magnetopause, *J. Geophys. Res.*, *112*, A09202, doi:10.1029/2007JA012419.

1. Introduction

[2] The magnetohydrodynamic (MHD) model of plasma physics allows the existence of three types of shocks: fast, slow, and intermediate. Initially in the study of MHD, it was largely agreed that intermediate shocks, though theoretically allowed, would be physically unrealizable for a variety of reasons [*Wu*, 2003]. For instance, the flow speed downstream of an intermediate shock is slow enough to allow intermediate wave perturbations to propagate upstream to the shock. Upstream of the shock, however, the flow speed is fast enough to prevent further propagation of the intermediate perturbation. It was then argued that such intermediate perturbations would cause a mismatch between upstream and downstream plasma conditions and would thus destabilize the intermediate shock [*Kantrowitz and Petschek*, 1966].

[3] However, work with dissipative MHD theory and simulation indicated that resistivity could stabilize the intermediate shock against intermediate wave perturbations [*Wu*, 1987, 1988, 1990]. Further, MHD intermediate shocks were discovered in MHD simulations of space physics systems. Solar coronal mass ejections were predicted to generate large shock fronts that are intermediate and stable at the nose of the shock [*Steinolfson and Hundhausen*, 1990a, 1990b, 1990c]. The morphology of these fronts was particularly surprising, being concave or "dimpled" at the nose. Simulations also showed stable intermediate shocks forming upstream of conducting, spherical, nonmagnetospheric obstacles such as the planet Venus, with the same concave morphology at the nose [*Steinolfson and Cable*, 1993]. Further simulations by De Sterck and Poedts extended these results to more generally ellipsoidal obstacles and fully three-dimensional geometries, demonstrated that these intermediate shocks form when solar wind conditions are right for forming switch-on shocks, and demonstrated that intermediate shocks can be destroyed and reformed by changing solar wind conditions [*De Sterck*, 1999; *De Sterck and Poedts*, 1999a, 2000, 2001]. In particular, simulation parameter surveys in the work of *De Sterck* [1999] showed that intermediate shocks will form upstream of a planetary barrier when solar wind conditions support the formation of switch-on shocks, those conditions being

$$\frac{2}{\gamma}\beta > 1$$

$$\rho v_n^2 > \frac{B^2}{4\pi} > \rho v_n^2 \frac{\gamma - 1}{\gamma(1-\beta)+1}$$

[1]Engineer Research and Development Center Major Shared Resource Center, U.S. Army Corps of Engineers, Vicksburg, Mississippi, USA.
[2]Department of Physics, Auburn University, Auburn, Alabama, USA.
[3]Department of Mechanical Engineering, Mississippi State University, Starkville, Mississippi, USA.

0148-0227/07/2007JA012419

*This title is correct as shown here. The article as originally published is online.

where all quantities are upstream of the shock and ρ is plasma density, γ is the polytropic index of the plasma, v_n is the velocity component normal to the shock front, and β is the plasma $\beta \equiv 8\pi B^2/p$, where B is the magnetic field magnitude and p is the pressure. (Since we are discussing switch-on shocks here, it is assumed that **B** is normal to the shock front.) The first of these inequalities states equivalently that the Alfvén velocity in the plasma must be greater than the sound speed, which is also equivalent to stating that the Alfvén Mach number must be smaller than the sound speed Mach number. The first part of the second inequality states that the flow speed must be super Alfvénic. The second part of the same inequality is more complicated but restricts the Alfvén Mach number to relatively low values. When the polytropic index γ is taken to be 5/3, as in our simulations, this inequality implies that the Alfvén Mach number must be smaller than 2.

[4] To our knowledge, the question of whether these intermediate shocks can form upstream of a magnetospheric obstacle, i.e., a dipole magnetic field rooted in a planetary body, has been so far left unaddressed. If there was no reconnection between the solar wind interplanetary magnetic field (IMF) and the magnetospheric field, the answer would probably be ''yes'': The magnetosphere would simply be a largely ellipsoidal obstacle to the solar wind and would produce intermediate shock configurations consistent with the accepted MHD simulations. However, one of the solar wind conditions needed to form intermediate bow shocks is an IMF pointing largely parallel to the solar wind flow, that is, largely sunward or largely antisunward. This situation makes the question more complicated. When the IMF points thus, the magnetic field in one hemisphere, either north or south, will be aligned largely parallel with the IMF, while the field in the opposite hemisphere will be aligned largely antiparallel to the IMF. In the hemisphere with the largely antiparallel field, some reconnection between the magnetospheric field and the IMF is to be expected. In the opposite hemisphere, we can expect little or none. This asymmetry in reconnection will produce some asymmetry in the conditions downstream of the shock. It is not clear a priori that these asymmetries will be trivial or that the intermediate shock configuration can form in the solar wind.

[5] An investigation of this question via three-dimensional MHD simulations will be presented in section 2. The simulation method and the results gathered will be discussed.

[6] The qualitative differences between the intermediate and typical fast bow shocks raise the question of what processes are important in the transformation of the bow shock from one type of shock to the other. We therefore study how the intermediate shock changes into a more standard fast shock under dynamic solar wind conditions. We launch a shock, constructed to remove the solar wind from the switch-on shock regime, into the upstream solar wind and observe its ensuing interaction with the bow shock, magnetosheath, and magnetosphere, paying particular attention to the MHD waves thus generated. In section 3 we present the results obtained from this dynamic study. We discuss some general conclusions from these results in section 4.

2. Steady-State Methodology and Results

[7] We study this problem with three-dimensional MHD simulations. The code we use solves the time-dependent MHD equations with an explicit time-stepping method that is second-order accurate in space and time. We discretize the MHD equations on a spherical grid with variable gridding in the radial direction. Shock capturing is accomplished with a small amount of artificial dissipation added to the MHD equations. Although we are mainly interested in simulating day side phenomena, our simulation domain spans the entire 4π steradians. This helps stabilize the simulation on the flanks, as well as improving the accuracy in that region. To ensure that our outer boundary lies beyond any intermediate shocks, which can extend rather far into the solar wind on the flanks [*Steinolfson and Cable*, 1993; *De Sterck and Poedts*, 2000], it is set to $80R_E$. The inner boundary is set at $6R_E$. $\nabla \cdot \mathbf{B}$ is kept small by periodically solving for and subtracting off the nonsolenoidal part of **B**. Added stability is gained by special treatment of the magnetic field. The initial field $\mathbf{B}_0$ is a potential field, and therefore force-free. This field can then be subtracted term by term from the MHD equations before finite differencing takes place, mitigating the detrimental effects of taking small differences between adjacent large values. For instance, in the $\mathbf{j} \times \mathbf{B}$ terms of the MHD momentum equations, instead of calculating finite differences of

$$\frac{1}{4\pi}\mathbf{j} \times \mathbf{B} \equiv \frac{1}{4\pi}\nabla \cdot (\mathbf{BB}) - \frac{1}{8\pi}\nabla B^2$$

we take finite differences on the mathematically and physically equivalent expression

$$\frac{1}{4\pi}\nabla \cdot (\mathbf{BB}) - \frac{1}{8\pi}\nabla B^2 - \frac{1}{4\pi}\nabla \cdot (\mathbf{B}_0\mathbf{B}_0) + \frac{1}{8\pi}\nabla B_0^2 = \frac{1}{4\pi}\nabla\cdot(\delta\mathbf{B}\mathbf{B}_0 + \mathbf{B}\delta\mathbf{B}) - \frac{1}{8\pi}\nabla((\mathbf{B} + \mathbf{B}_0) \cdot \delta\mathbf{B})$$

where $\delta\mathbf{B} = \mathbf{B} - \mathbf{B}_0$.

[8] Our numerical scheme has four free dimensionless parameters: the solar wind sound speed mach number, $M_s \equiv v_0/C_s$, the angle between the solar wind velocity and magnetic field, the strength of the magnetospheric dipole expressed in terms of the solar wind magnetic field and inner simulation radius, and the solar wind plasma $\beta \equiv 8\pi p_0/B^2{}_0$, where p_0 is the solar wind thermal pressure and B_0 is the solar wind magnetic field strength. All of the simulation quantities can be expressed in terms of these quantities, so the results of the simulation can be subject to interpretation based on normalization. We chose $M_s = 2.2$ and $\beta = 0.39$. The magnetic field points sunward, i.e., antiparallel to the flow direction. (If we were to orient the field antisunward, the results of our simulation would be the same, just reflected across the equatorial plane.) These parameters are all suitable for producing switch-on and intermediate shocks. Table 1 lists values of the dimensional

Table 1. Solar Wind Simulation Parameters, Given Normalization Appropriate to Magnetospheric Phenomena[a]

Solar Wind Quantity	Value
n	1.0 cm^{-3}
T	5.7×10^{5}°K
B	10^{-5} nT
v	275 km/s
C_s	125 km/s
V_A	218 km/s
M_s	2.20
M_A	1.26
β	0.39
μ_E	8×10^{15} T-m^3

[a]Here n represents H^+ number density, T is temperature, B is magnetic field strength, v is velocity, C_s is sound speed, V_A is Alfvén speed, M_s is the sonic Mach number, M_A is the Alfvén Mach number, β is the plasma beta, and μ_E is the terrestrial dipole moment.

solar wind parameters, assuming a normalization appropriate to magnetospheric phenomena.

[9] We proceed by setting initial conditions and then letting the simulation run to steady state in the dayside. The initial magnetic field in the domain is a sum of the terrestrial field and the uniform field of the upstream solar wind. The velocity is zero near the inner boundary and in the nightside; on the dayside, it ramps up to the chosen solar wind velocity several R_E outside the magnetosphere. In this simulation, the average radial grid spacing through the magnetosphere and magnetosheath is $0.15R_E$. θ grid spacing is uniform at 2.5 degrees; azimuthal grid spacing is uniform at 4.75 degrees.

[10] For comparison, we also run a simulation with similar solar wind conditions but with simple hard shell boundary conditions on the inner boundary. With these simpler conditions, the inner boundary can be interpreted as the ionosphere of a nonmagnetic planet such as Venus or as a very rough approximation to the magnetopause of a planetary magnetosphere. In this simulation, the average radial grid spacing in the magnetosheath is about 0.003 times the radius of the spherical obstacle, which translates into $0.03R_E$, if we interpret the inner sphere as a crude representation of the magnetosphere. Angular gridding is the same as in the previous magnetospheric simulation.

[11] Figure 1 shows density contours and magnetic field lines obtained when the simulation reaches steady state. For reference, Figure 1a shows the density and field lines obtained in the simpler simulation where the inner boundary is a hard spherical shell representing the magnetopause at a radius of $10R_E$. The bow shock formed by this spherical magnetopause inner boundary shows a distinct MHD intermediate shock region surrounding the nose of the shock. This is most clearly seen by examining the behavior of the magnetic field lines as they cross the shock front. Since the tangential component of the magnetic field must switch signs across an MHD intermediate shock, the field lines will remain on the same side of the shock normal as they cross the shock front. In contrast, the field lines of all other MHD shocks will cross the shock normal as they cross the front. Figures 1b–1d show density contours and magnetic field lines with a more physical dipole field magnetosphere. Figure 1b shows the configuration obtained in the equatorial plane. Note that, as in the simpler magnetopause simulation, field lines near the nose remain on the same side of the shock normal as they cross the shock, though this behavior is not nearly as pronounced. The shock in the equatorial plane is, then, marginally intermediate, very similar to a switch-on shock. The simulation gridding for the simulations has been discussed above. In both cases, the shock spans about 5 grid points on the Sun-Earth line.

[12] In the noon-midnight meridian plane (Figure 1c and the enlargement in Figure 1d), the situation is more complex. Figure 1c shows density and magnetic field lines in the noon-meridional plane, while Figure 1d shows an enlargement of Figure 1c at the nose of the shock, specifically GSE x between 18 and $22R_E$ and GSE z between -10 and $10R_E$. The lines "A" and "B" drawn on Figure 1d cross the bow shock perpendicular to the shock at their respective locations. It can be seen that the magnetic field lines near "A," in the southern hemisphere, "reflect" at "A" as they cross the shock. In contrast, the lines near "B," in the northern hemisphere, cross "B" as they cross the shock. This means that the shock near "A" is intermediate, while the shock near "B" must be a regular fast shock.

[13] We wish to discuss the cause of the the contrast between the shock configurations in the northern and southern hemispheres, but a few comments on the overall structure, with particular regard to the standoff distance, are in order first. Given the relatively low Mach numbers of the solar wind, the reader might find the relative shock standoff distances to be surprisingly short in both simulations. After all, under more typical solar wind conditions with substantially higher Mach numbers, the magnetopause radius is generally in the neighborhood of $10R_E$, with the distance to the shock front being another $4R_E$, a full 40 percent of the size of the magnetosphere. It is certainly to be expected that the relative standoff distance would grow and not shrink with smaller solar wind mach numbers. Indeed, this expectation has been confirmed by numerous studies conducted or simulated in normal solar wind conditions but not in conditions capable of generating switch-on and intermediate shock fronts. In fact, studies carried out in the switch-on shock regime produce standoff distances consistent with the short distances we have found here, despite their counterintuitive character [*Steinolfson and Cable*, 1993; *De Sterck*, 1999; *De Sterck and Poedts*, 1999a, 2000, 2001]. Further, parameter studies have shown that the standoff distances of bow shocks formed in the switch-on shock regime are not only smaller than might be intuitively expected but actually decrease with decreasing solar wind Mach number, because of the increase of the "dimpling" at the shock nose as the Mach number drops [*Cairns and Lyon*, 1996; *De Sterck and Poedts*, 1999b; *Chapman et al.*, 2004].

[14] In Figure 1a, the distance from the spherical obstacle (which has been assigned a radius of $10R_E$ for illustrative purposes) to the shock front is only about one tenth of the radius of the obstacle. In Figures 1b and 1c, the distance on the Sun-Earth line from the magnetopause to the shock front is about one quarter of the radius of the magnetopause. This contrast in relative shock thickness arises because the more realistic magnetopause in Figures 1b and 1c is a more blunt obstacle than the spherical inner boundary in Figure 1a. Specifically, note that in the equatorial plane (Figure 1b), the magnetopause radius is about $16R_E$ on the Sun-Earth line, but closer to $19R_E$ on the flanks.

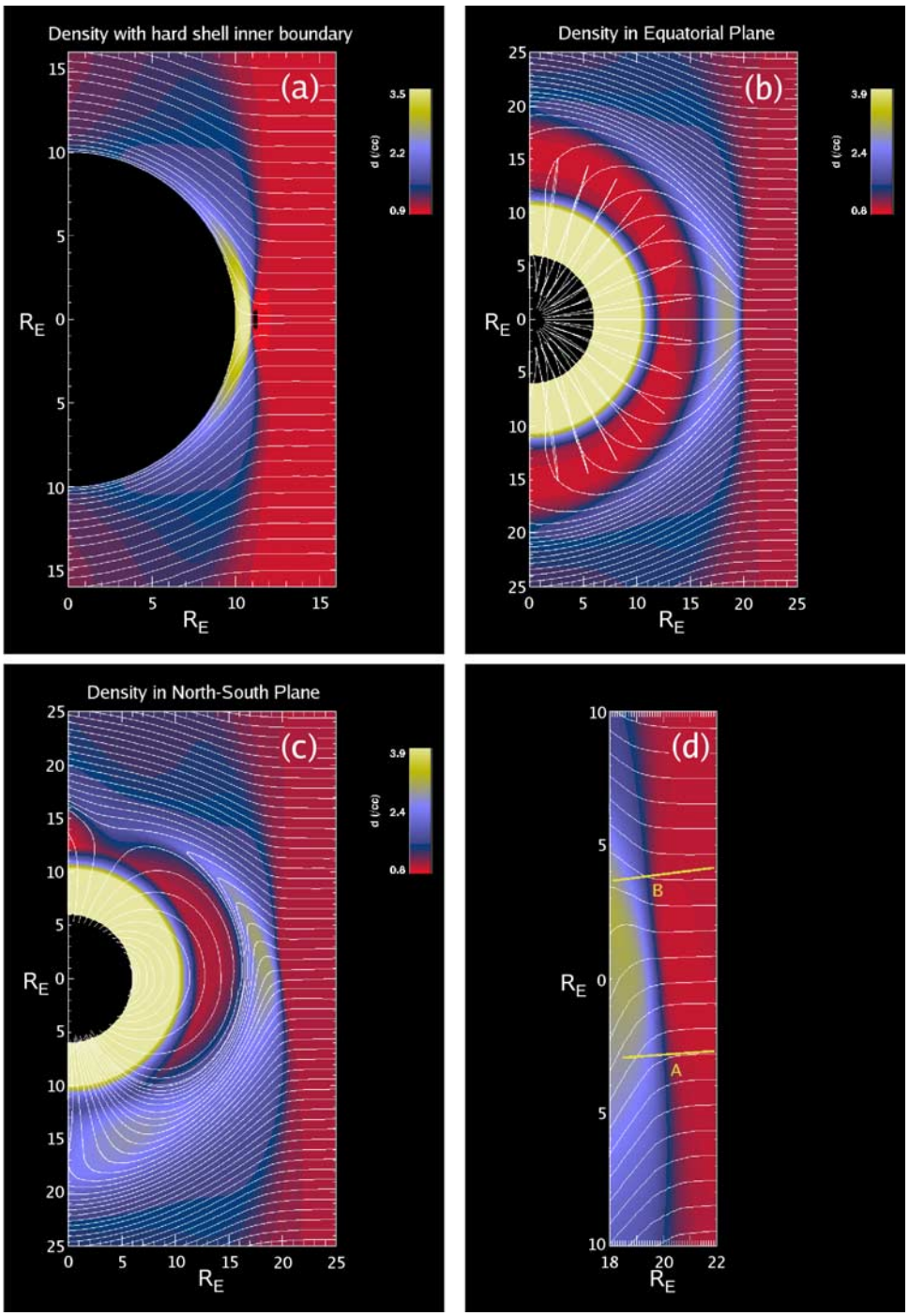

Figure 1. Density contours and magnetic field lines in the magnetospheric simulation in (a) a simulation with a simple hard shell inner boundary representing the magnetopause at $10R_E$, (b) the equatorial plane of the magnetospheric simulation, and (c) in the noon-midnight meridional plane of the magnetospheric simulation. Also shown is (d) an enlargement of Figure 1c in the region $x = [18R_E, 22R_E]$ and $z = [-10R_E, 10R_E]$. Note that at location A, in the southern hemisphere, magnetic field lines "reflect" across the shock normal when they cross the shock surface, indicating an MHD intermediate shock. At location B, they cross the shock normal, indicating an MHD fast shock.

[15] With regard to the contrast in shock characteristics between the northern and southern hemispheres, this difference can be attributed to magnetic reconnection at the magnetosphere. Magnetic field lines in the northern hemisphere have much stronger curvature than in the southern hemisphere. This curvature is the effect of magnetic reconnection between the IMF and the terrestrial magnetic field, occurring almost entirely in the northern hemisphere where the two fields are largely antiparallel. To reach a steady state, the northern hemisphere magnetosheath plasma

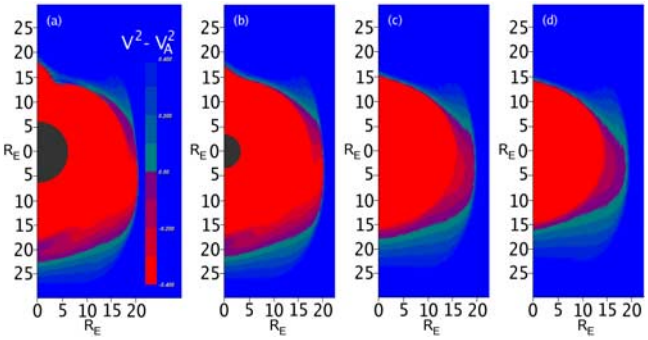

Figure 2. Contours of $V^2 - V_A{}^2 < 0$ in planes parallel to the noon-midnight meridional plane (i.e., the GSE x-z plane), showing (a) the noon-midnight plane, (b) displaced laterally (in GSE y) $5R_E$ from the noon-midnight plane, (c) $10R_E$ from the noon-midnight plane, (d) and $12R_E$ from the noon-midnight plane.

requires a more complex configuration of pressure and density to counteract the force of the magnetic tension. A different shock structure is then produced in the northern hemisphere: A standard MHD fast shock takes the place of the intermediate shock. This seems to be a unique case of reconnection at the magnetosphere affecting global magnetosheath and bow shock characteristics. We may surmise that these effects are possible because, in this case, the earthward solar wind flow speed is relatively slow compared with the speed that is seen in the typical fast shock case. Therefore information can propagate much more effectively from the magnetosphere into the magnetosheath and bow shock. In this particular simulation, because of inhomogeneities in the plasma near the magnetopause, the reconnection inflow velocity is difficult to determine with great accuracy. However, in the reconnection region in the $y = 0$ plane, near the center of the X-line, the data indicate that the normal inflow velocity relative to the Alfvén speed, v_N/V_A, is close to 0.05 ± 0.02, somewhat lower than the generally accepted rate of $\sim$0.1. Although we do not claim that this is the "correct" magnetopause reconnection rate, it is worth pointing out that the reconnection observations of *Fuselier et al.* [2005] from Cluster also indicate an inflow velocity substantially lower than 0.1, specifically $v_N/V_A \leq 0.02$.

[16] Figure 1 gives an idea of the characteristics of the bow shock only in two planes. The question arises: What is the global three-dimensional structure of the bow shock and where, in general, does it take on an intermediate character on the one hand and a fast character on the other? To answer this question, we can make use of another unique property of intermediate shocks.

[17] On the one hand, upstream of an intermediate shock, the plasma flow speed normal to the shock front, V_n, is greater than the component of the intermediate (or Alfvén) wave speed normal to the shock front, V_{An}: $V_n > V_{An}$. On the other hand, downstream of the shock, $V_{An} > V_n$. So we can examine the difference between the normal components of the flow and intermediate wave speeds immediately behind the shock to determine the type of shock across the various regions of the bow shock. Where $V_{An} > V_n$, the shock is intermediate. This examination is made simpler because our solar wind magnetic field and velocity are aligned in exactly opposite directions, as discussed above. Therefore the shock frame of reference is a de Hoffmann-Teller (HT) frame. In an HT frame, $V/V_A = V_n/V_{An}$. Therefore $V_{An} > V_n$ if and only if $V_A > V$. We can therefore simply examine the plasma and intermediate velocity magnitudes behind the shock.

[18] Figures 2a–2d show contours of the quantity $V^2 - V_A^2$. The contours are taken in planes parallel to the noon-midnight meridional plane (i.e., the GSE x-z plane). Figure 2a shows values in the $y = 0$ plane, Figure 2b in the $y = 5R_E$ plane, Figure 2c in the $y = 10R_E$ plane, and Figure 2d in the $y = 12R_E$ plane. To establish where the shock is intermediate, we look just behind the shock for areas where $V^2 - V_A^2 < 0$. (Figure 2 is plotted so that $V^2 - V_A^2 < 0$ is shown as red-violet and $V^2 - V_A^2 > 0$ is shown as blue-green. Note that in the interior of the magnetosheath and magnetosphere, the flow speed will continue to decrease while the Alfvén speed will remain finite or even increase. Therefore much of the interior space of Figure 2 is colored red. The important behavior for present purposes is that occurring just behind the shock.) In Figure 2a, it can be seen that in the northern hemisphere, the shock is intermediate at the equator. Immediately north of the equator, it is marginally intermediate and changes to a standard fast shock somewhere between 2 and $5R_E$ north of the equator. In the southern hemisphere, the shock is clearly intermediate from the equator down to about $12R_E$ south of the equator. In Figure 2d, it can be seen that $V^2 - V_A^2 > 0$ everywhere immediately behind the shock. Therefore the bow shock is purely an MHD fast shock for $y = 12R_E$ and greater. The intermediate shock, then, occupies an area on the bow shock surface located largely in the southern hemisphere and extending laterally about $12R_E$ out on the flanks of the shock. It is true that the bow shock takes on the character of an MHD fast shock in regions of both the northern and southern hemispheres. This is to be expected. As we follow the intermediate shock from the equator northward or southward, we will eventually reach a point where the shock becomes a switch-on shock. Moving further beyond the equator from that point, either north or south, we will find that the shock is an MHD fast shock. This situation is established also in the case of the simple hard shell inner boundary (not shown here). The salient point is that in the magnetospheric case shown in Figure 2, the intermediate shock is located largely in the southern hemisphere, in contrast to the simple hard shell case, where it is distributed in a cylindrically symmetric manner around the Sun-Earth line.

3. Dynamic Interaction Between Bow Shock and Solar Wind Disturbance

[19] We now investigate the dynamic behavior of the intermediate bow shock in interaction with a shock propagating downstream in the solar wind. The shock's parameters are selected so that the shock will move the solar wind out of the switch-on shock regime and will therefore change the bow shock into a typical fast shock.

[20] Into our steady-state configuration of the previous section, we launch a fast solar wind shock. This shock disturbance in the solar wind is oriented to propagate toward the Earth (i.e., the propagation direction points in GSE $-\hat{x}$),

Table 2. Solar Wind Parameters of Fast Shock Disturbance[a]

Solar Wind Quantity	Value
n	2.87 cm^{-3}
T	1.84×10^{6}°K
B	10^{-5} nT
v	500 km/s
C_s	125 km/s
V_A	218 km/s
M_s	2.22
M_A	3.8
β	3.6

[a]Here n represents H^+ number density, T is temperature, B is magnetic field strength, v is velocity, C_s is sound speed, V_A is Alfvén speed, M_s is the sonic Mach number, M_A is the Alfvén Mach number, β is the plasma beta, and μ_E is the terrestrial dipole moment.

with parameters behind this new shock as given in Table 2. This shock effects a sudden change in the solar wind density, temperature, and flow speed. Behind this new shock, the Alfvén Mach number and plasma β take on new values such that the Alfvén speed is now slower than the sound speed, or alternatively, the Alfvén Mach number is greater than the sonic Mach number. These changes throw the solar wind into a regime where switch-on shocks and intermediate shocks cannot be supported. In the ensuing interaction, the bow shock ahead of the magnetosphere changes to a typical fast shock.

[21] The important stages of the interaction between the new shock and the magnetospheric bow shock from Figures 1b–1d are shown in Figure 3. Figure 3a shows density; Figure 3b shows V_x. (Note that x points sunward, so V_x is largely negative.) The view is in the noon-midnight meridional plane. At about 0.5 min after the simulation begins, the solar wind shock disturbance makes contact with the bow shock. A fast shock begins to propagate through the magnetosheath. Behind this fast shock, both the bow shock and magnetopause begin moving inward toward the Earth. After about 3.5 minutes, the fast shock reaches the inner boundary. Another fast disturbance, more accurately characterized as a fast wave than a fast shock, reflects from the inner boundary. It crosses the magnetopause about 5 min into the simulation and reaches the bow shock about 1 min after that. When it reaches these two interfaces, it stops their motion on the Sun-Earth line. The flanks then adjust to the new solar wind conditions. After about 10 min into the simulation, the dayside has reached a new equilibrium.

[22] Figure 4 shows more continuous views of the evolution of V_x (Figure 4a) and entropy (Figure 4b) along the Sun-Earth line. All of the above features of the interaction can be seen clearly in the V_x plots. In the entropy plots, however, the reflected fast disturbance is only barely discernable. We conclude, as stated immediately above, that this reflected disturbance is a fast wave and not a fast shock.

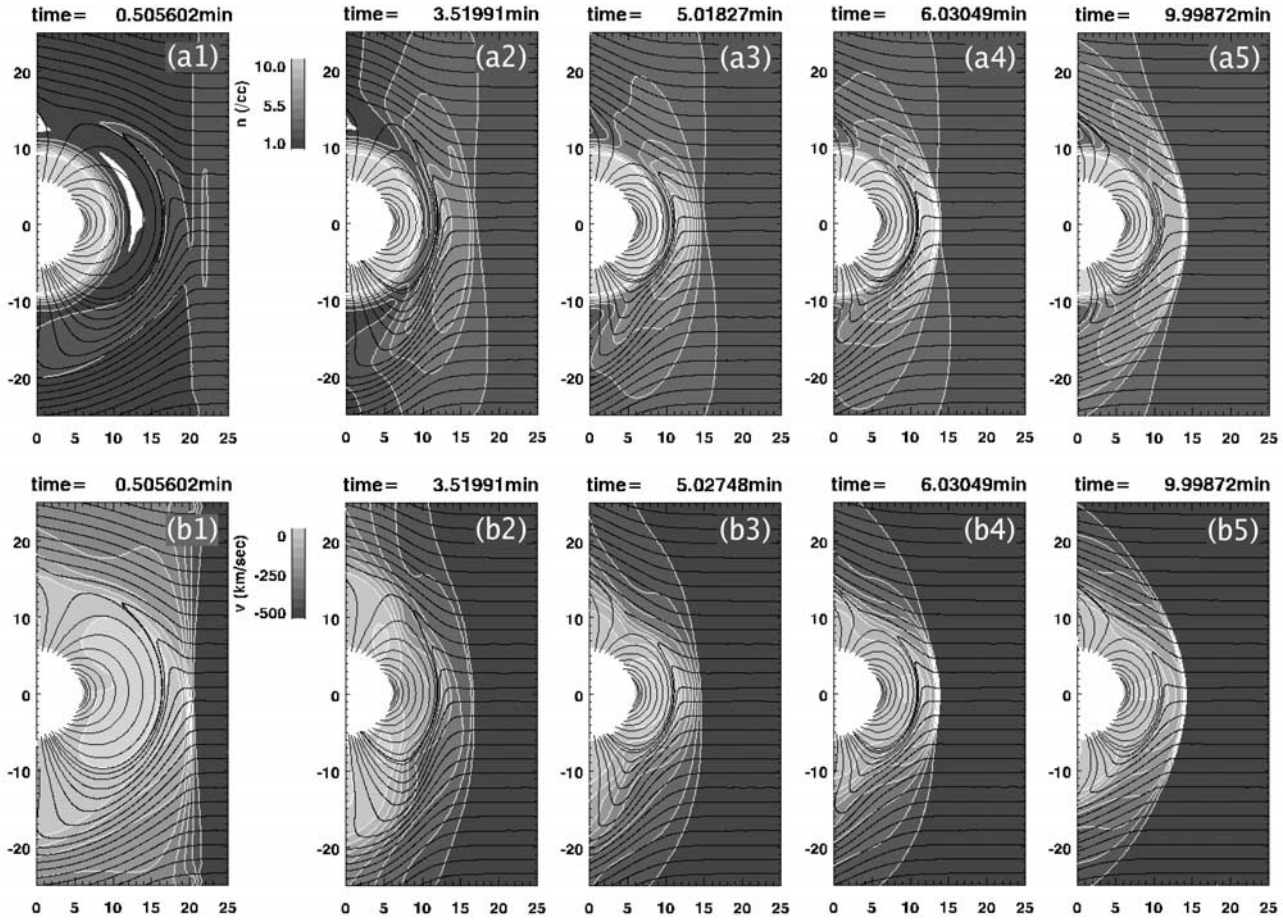

Figure 3. Time evolution of bow shock/fast shock interaction, showing (a) density and magnetic field lines and (b) V_x and magnetic field lines.

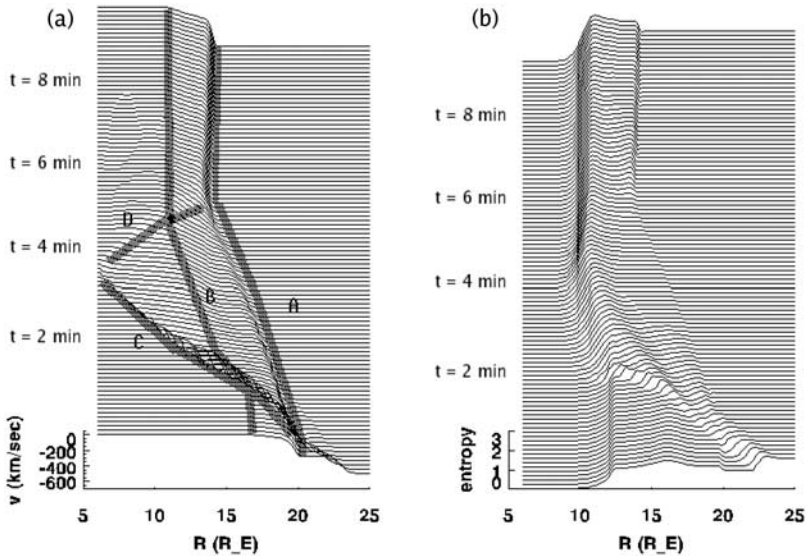

Figure 4. The time sequence of (a) V_x and (b) entropy, along the Sun-Earth line. Figure 4a is annotated with guides to the eye marking the movement of (A) the bow shock, (B) the magnetopause, (C) the transmitted fast shock, and (D) the reflected fast wave. Note that the transmitted fast shock causes a notable disturbance in entropy, in contrast to the reflected fast wave.

The reader might notice that the magnetopause and bow shock stop their inward motion almost immediately upon contact with the reflected fast wave. We believe this effect is real but is probably not typical of this type of interaction and is a fortuitous consequence of the particular simulation parameters. In simulations run by ourselves in other contexts, it is seen that the reflected fast wave pushes the magnetopause and bow shock out into the solar wind beyond their equilibrium positions by a few Earth radii; the magnetopause and bow shock then asymptote inward to their equilibrium values [*Cable and Lin*, 2005].

[23] Two qualifying comments are in order here. First, the temperature of the solar wind behind the fast shock, $1.84 \times 10^{6\circ}$K, is higher than will be observed in the physical solar wind. This shock was picked in order to satisfy the Rankine-Hugoniot conditions between the original and disturbed solar wind, and to immediately move the solar wind plasma into a state where it would not support intermediate shocks. Interactions of the intermediate bow shock with other types of disturbances, such as might involve rotation of the magnetic field, are also of interest and will be the subject of future work. Also, we recognize that the timing of the fast reflection is distorted by having our inner boundary at $6R_E$ instead of a more physically realistic $3R_E$. However, this difference should not affect in any qualitative sense the results we have presented here.

4. Conclusions

[24] We have shown that a magnetized body such as the Earth can sustain the type of intermediate solar wind shocks that have been simulated in relation to solar prominences and nonmagnetized bodies. Important qualitative differences arise between the shocks produced by nonmagnetized and magnetized bodies, however. Intermediate shocks will form only for small cone angles of the IMF. That is, the IMF must be pointing largely toward or away from the magnetospheric obstacle. Under such conditions, differences in magnetic reconnection between the northern and southern hemispheres will produce a bow shock with very different characteristics in the northern and southern hemispheres. In the hemisphere with little reconnection (southern, in our case), the bow shock will have intermediate shock characteristics very similar to what has been seen in conjunction with nonmagnetized bodies. In the opposite hemisphere, however, distortion of the IMF through magnetic reconnection will force the bow shock into a more typical fast shock configuration. Reconnection at the magnetosphere can therefore affect significantly the structure of the upstream magnetosheath and bow shock. This state of affairs stands in contrast to the bow shock produced under typical fast shock conditions. We surmise that these effects can occur because in the low solar wind speeds we deal with here, disturbances from the magnetopause can propagate much more effectively upstream toward the bow shock.

[25] We have also investigated an interaction with a solar wind disturbance that erases the intermediate character of the bow shock. The changes in the bow shock, magnetosheath, and magnetosphere are produced almost entirely by a transmitted fast shock that propagates to the lower magnetosphere and is then reflected as a much weaker fast wave. Interactions with other types of solar wind disturbances, such as shocks involving rotation of the IMF, or perhaps entropy discontinuities, are also of interest and will be the subject of future research. Also, the magnetospheric dipole tilt angle is likely to have a strong effect on the location and extent of the intermediate shock region; a study of this effect will also be researched.

[26] **Acknowledgments.** Computer time for this work was provided by the U.S. Army Engineer Research and Development Center Major Shared Resource Center (ERDC MSRC) and the Department of Defense High Performance Computing Modernization Program.

[27] Zuyin Pu thanks Steven Petrinec and another reviewer for their assistance in evaluating this paper.

References

Cable, S., and Y. Lin (2005), The MHD intermediate magnetosheath as affected by solar wind MHD disturbances and magnetospheric reconnection., *Eos Trans. AGU*, *86*(52), Fall Meet. Suppl., Abstract SM51B–1303.

Cairns, I. H., and J. G. Lyon (1996), Magnetic field orientation effects on the standoff distance of the Earth's bow shock, *Geophys. Res. Lett.*, *23*, 2883–2886.

Chapman, J. F., I. H. Cairns, J. G. Lyon, and C. R. Boshuizen (2004), MHD simulations of Earth's bow shock: Interplanetary magnetic field orientation effects on shape and position, *J. Geophys. Res.*, *109*, A04215, doi:10.1029/2003JA010235.

De Sterck, H. (1999), Numerical simulation and analysis of magnetically dominated MHD bow shock flows with applications in space physics, Ph.D. dissertation, Katholieke Univ. Leuven, Leuven, Belgium.

De Sterck, H., and S. Poedts (1999a), Stationary slow shocks in the magnetosheath for solar wind conditions with $\beta < 2/\gamma$: Three-dimensional MHD simulations, *J. Geophys. Res.*, *104*, 22,401–22,406.

De Sterck, H., and S. Poedts (1999b), Field-aligned magnetohydrodynamic bow shock flows in the switch-on regime, *Astron. Astrophys.*, *343*, 641–649.

De Sterck, H., and S. Poedts (2000), Intermediate shocks in three-dimensional magnetohydrodynamic bow-shock flows with multiple interacting shock fronts, *Phys. Rev. Lett.*, *84*(24), 5525–5527.

De Sterck, H., and S. Poedts (2001), Disintegration and reformation of intermediate-shock segments in three-dimensional MHD bow shock flows, *J. Geophys. Res.*, *106*, 30,023–30,037.

Fuselier, S. A., K. J. Trattner, S. M. Petrinec, C. J. Owen, and H. Réme (2005), Computing the reconnection rate at the Earth's magnetopause using two spacecraft observations, *J. Geophys. Res.*, *110*, A06212, doi:10.1029/2004JA010805.

Kantrowitz, A., and H. Petschek (1966), *Plasma Physics in Theory and Application*, McGraw-Hill, New York.

Steinolfson, R. S., and S. Cable (1993), Venus bow shocks at unusually large distances from the planet, *Geophys. Res. Lett.*, *20*, 755–758.

Steinolfson, R. S., and A. J. Hundhausen (1990a), MHD intermediate shocks in coronal mass ejections, *J. Geophys. Res.*, *95*, 6389–6401.

Steinolfson, R. S., and A. J. Hundhausen (1990b), Concave outward slow shocks in coronal mass ejections, *J. Geophys. Res.*, *95*, 15,251–15,256.

Steinolfson, R. S., and A. J. Hundhausen (1990c), Coronal mass ejection shock fronts containing the two types of intermediate shocks, *J. Geophys. Res.*, *95*, 20,693–20,699.

Wu, C. (1987), On MHD intermediate shocks, *Geophys. Res. Lett.*, *14*, 668–671.

Wu, C. (1988), The MHD intermediate shock interaction with an intermediate wave: Are intermediate shocks physical?, *J. Geophys. Res.*, *93*, 987–990.

Wu, C. (1990), Formation, structure, and stability of MHD intermediate shocks, *J. Geophys. Res.*, *95*, 8149–8175.

Wu, C. (2003), MKDVB and CKB shock waves, *Space Sci. Rev.*, *107*, 403–421.

S. Cable, Engineer Research and Development Center Major Shared Resource Center, U.S. Army Corps of Engineers, CEERD-IH, 3909 Halls Ferry Rd., Vicksburg, MS 39183, USA. (sam.b.cable@erdc.usace.army.mil)

J. L. Holloway, Department of Mechanical Engineering, Mississippi State University, Starkville, MS 29762, USA. (jlh530@msstate.edu)

Y. Lin, Department of Physics, Auburn University, 206 Allison Laboratories, Auburn, AL 36849, USA. (ylin@physics.auaburn.edu)